Finite element method coupled with a numerical cellular automaton model to simulate the residual stress of dual phase DP600 steel Nd:YAG laser welding

Shibo Liu, Adinel Gavrus, Afia Kouadri-Henni

Finite element method coupled with a numerical cellular automaton model used to simulate the residual stresses of dual phase DP600 steel Nd:YAG laser welding

S. LIU[a], A. GAVRUS[b]*, A. KOUADRI-HENNI[c]

a. Bretagne Loire University (UBL), INSA Rennes, LGCGM (EA 3913), 20 Avenue des Buttes de Cöesmes, 35708, Rennes, France, email : shibo.liu@insa-rennes.fr
b. Bretagne Loire University (UBL), INSA Rennes, LGCGM (EA 3913), 20 Avenue des Buttes de Cöesmes, 35708, Rennes, France, email : adinel.gavrus@insa-rennes.fr
c. Bretagne Loire University (UBL), INSA Rennes, LGCGM (EA 3913), 20 Avenue des Buttes de Cöesmes, 35708, Rennes, France, email : afia.kouadri-henni@insa-rennes.fr

Résumé :

Un modèle thermo-mécanique couplé séquentiellement a été développé pour étudier les contraintes résiduelles de l'acier double phase DP600 soudé par un procédé au laser Nd: YAG. Un modèle d'automate cellulaire numérique (CA) a d'abord été construit pour simuler l'évolution de la microstructure lors d'un soudage au laser. Les résultats d'orientation de la microstructure CA obtenus sont entrés dans un modèle d'éléments finis (FEM) pour décrire l'anisotropie élastique avec une loi constitutive correspondante caractérisant le comportement thermo-mécanique du matériau en prenant en compte l'écrouissage de la ferrite-martensite à double phase, la sensibilité à la température et l'influence de la vitesse de déformation. L'analyse des contraintes résiduelles numériques prédites par le modèle couplé CA-FEM montre une légère sensibilité à la vitesse de déformation.

Abstract :

A sequentially coupled thermo-mechanical model has been developed to investigate the residual stresses of DP600 dual phase steel welded by a Nd:YAG laser process. A numerical cellular automaton (CA) model has been firstly built to simulate the microstructure evolution during a laser welding. The obtained CA microstructure orientation results are input into a finite element model (FEM) to describe elasticity anisotropy together with a corresponding constitutive law characterizing the thermo-mechanical material behavior taking into account the dual phase ferrite-martensite hardening, the temperature sensitivity and the strain rate influence. Analysis of numerical residual stresses predicted by the proposed coupled CA-FEM model show some influences of strain rate.

Key words : laser welding, dual phase DP600 steel, anisotropy, strain rate sensitivity, residual stresses

1 Introduction

To reduce energy consumption and CO_2 release, high strength alloy is widely used in automotive industries to reduce the car weight [1]. Among the high strength low weight alloys, the dual-phase (DP) steel possesses adequate ductility and high strength. DP600 contains about 15% hard martensite in a soft ferrite matrix [2]. The body-centered-tetragonal martensite helps to improve the high strength while the body-centered-cubic ferrite contributes to ductility [3]. The high strain-hardening rate can increase absorption energy in car collision, thus helps to decrease damage [4]. As is seen in figure 1, when the laser is focused on DP600 steel, the weld area absorbs energy rapidly and fused locally. Three areas of Fusion Zone (FZ), Heat Affected Zone (HAZ) and Base Metal (BM) are used to stand for different welding zone. The heated weld area expands but is compressed by the surrounding colder area. If the obtained stress exceeds the low yield strength corresponding to high temperature of material, the weld part is plastically hot-compressed. After cooling down, the weld part is too small relative to surrounding colder part. Thus, laser welding usually produces tensile residual stresses on the weld region and compressive residual stresses on the surrounding area. Many studies were conducted on dual-phase DP600 steel behavior, however concerning welding simulation of residual stresses there are not many precise material models for a numerical analysis. It is unclear how much DP600 elastic and plastic material properties will influence the yield strength and consequently the residual stresses of a laser welding simulation. Thus the main purpose of this study is to analyses more precisely the DP600 thermo-mechanical constitutive model, especially in order to evaluate the influence of the elastic and plastic anisotropy together with the strain rate sensitivity on simulated welding residual stresses.

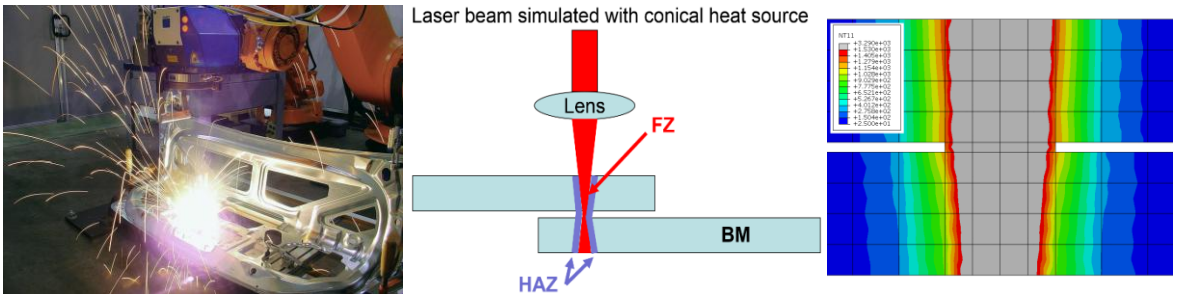

(a) (b) (c)

Figure 1. a) Laser welding process used by automotive industry [5]; b) The three laser welding zones (FZ-Fusion Zone, HAZ-Heat Affected Zone, BM-Base Metal); c) FE results of thermal gradients (FZ: grey part T > 1530°C, HAZ: from red to green part 25°C < T < 1530°C, BM: blue part T = 25°C)

2 CA Model – FEM Coupling

In the case of the deep penetration welding simulation, a conical heat source model with Gaussian distribution is used and the thermal flux Q_v is expressed from the laser power P and the efficiency factor η by:

$$Q_v(r,z)=\frac{9\eta Pe^3}{\pi(e^3-1)}\times\frac{e^{-\frac{3r^2}{r_c^2}}}{(z_e-z_i)(r_e^2+r_e r_i+r_i^2)} \quad (1)$$

Where the conical surface radius r_c is defined by:

$$r_c = r_i + \frac{(r_e - r_i)(z - z_i)}{z_e - z_i} \quad (2)$$

The shape of heat source, energy distribution and all variables of Eq. 1 and 2 are presented in figure 2.

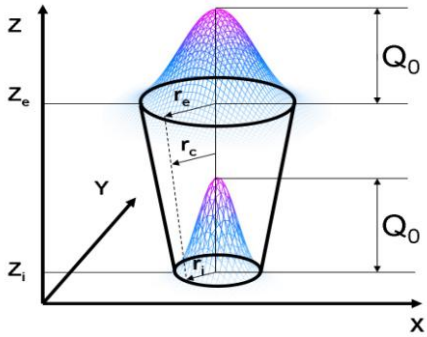

Figure 2. Gauss heat distribution of a conical heat source

The geometry, mesh and boundary condition of the laser welding thermos-mechanical model are pictured in figure 3. The path transversal to the weld line, the rolling direction and the directions of residual stresses estimation are also illustrated. The angle between transversal path and rolling direction is θ. A finite element model with 44160 C3D8R elements is selected for an Abaqus numerical analysis where all the dimensions are defined according to experimental data.

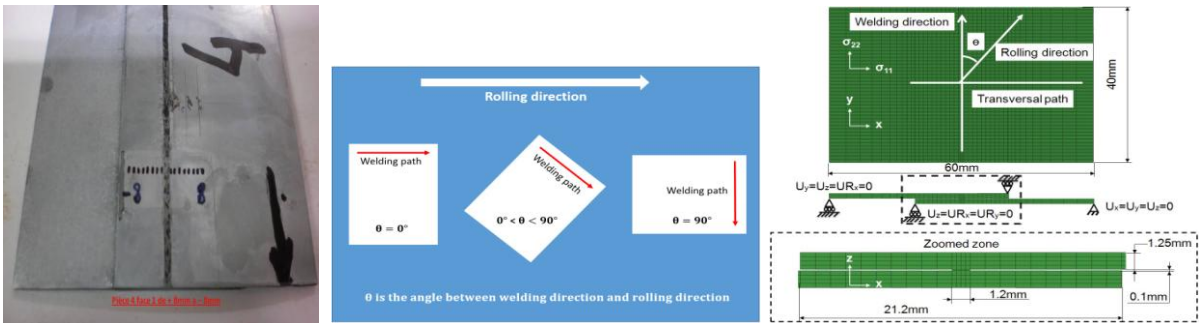

(a) (b) (c)

Figure 3. Experimental plates welding and ABAQUS/FEM numerical model: a) experimental plate welding along the rolling direction; b) Plates cut and welding patch using different orientations with respect to the rolling direction; c) Geometry and boundary conditions

The flowchart of used CA-FEM coupled model to simulate the residual stresses is shown figure 4. Based on the CA model the crystalline orientation and orientation fraction are firstly computed. Starting from these data, using an initial estimation of martensitic elastic constants are computed the corresponding weld orthotropic elastic constants used in a second step into the ABAQUS/FEM simulation of the laser welding process to estimate the residual stresses distribution.

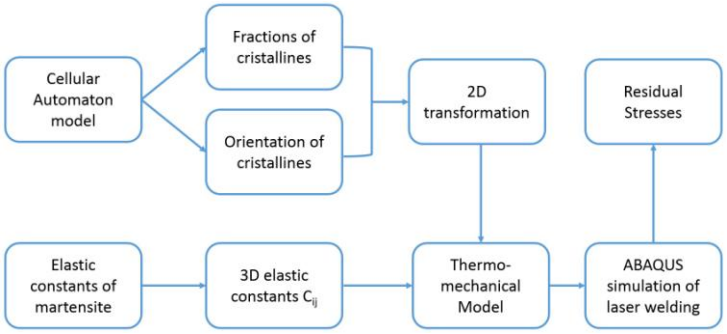

Figure 4. The flowchart of the CA-FE model used to simulate residual stresses

3 Anisotropy of dual-phase DP600 steel

The anisotropy of dual phase DP600 steel has been analyzed both from the solidification process using the numerical CA model and from the base metal thermo-mechanical behavior using a sequentially coupled thermal-elastic-plastic model and a plane anisotropy theory. It is observed that the residual stress longitudinal to welding direction is more influenced by the material anisotropy and the temperature sensitivity. The analysis of a coupled anisotropy model consists to take into account the anisotropy of weld and the anisotropy of base metal.

3.1 Analysis of weld elastic anisotropy

3.1.1 Base metal elasticity

For a rigorous computation of the residual stresses, the thermo-elasticity properties of DP600 base metal has an important influence, so the temperature influences are firstly considered to describe variations of the Young's modulus and Poisson's ratio (Table 1).

Table 1. Young's Modulus and Poisson's ratio of DP600 steel

Temperature (°C)	0	300	600	800
Young's Modulus (GPa)	210	190	120	30
Poisson's ratio	0.280	0.295	0.310	0.330
Thermal expansion coefficient	1.2×10^{-5}	1.5×10^{-5}	1.6×10^{-5}	1.6×10^{-5}

3.1.2 Weld material elasticity

Because of the high cooling rate of laser welding, during the solidification process the face centered cubic austenite of DP600 weld turns to body centered tetragonal martensite. This phase transformation phenomenon has been observed by many previous experimental works [6,7]. Due to the phase transformation and due to the the grain size decrease, the mechanical properties of the weld material are changed, such as observed by measurements of micro-hardness [8,9]. N.Farabi et al. [10] have investigated laser welding on DP600/DP980 steels and show that full martensite is found at FZ part (Fusion Zone). In this work the elastic constants of DP600 weld martensite are assumed to be the same with those of a martensitic steel [11]. If an orthotropic elastic anisotropy is considered, the martensitic elastic compliance S_{ij} which express the relationships between the elastic strain Voigth vector and the Cauchy stress Voigth vector can be computed by:

$$S_{ij} = C_{ij}^{-1} = \begin{bmatrix} \frac{1}{E_1} & \frac{-\nu_{21}}{E_2} & \frac{-\nu_{31}}{E_3} & & & \\ \frac{-\nu_{12}}{E_1} & \frac{1}{E_2} & \frac{-\nu_{32}}{E_3} & & & \\ \frac{-\nu_{13}}{E_1} & \frac{-\nu_{23}}{E_2} & \frac{1}{E_3} & & & \\ & & & \frac{1}{G_{12}} & & \\ & & & & \frac{1}{G_{13}} & \\ & & & & & \frac{1}{G_{23}} \end{bmatrix} \quad (3)$$

Starting from results obtained in [11] the following values are taking into account to describe elastic

anisotropy of the initial DP600 martensite:

$$C_{ij} = \begin{bmatrix} 268.1 & 111.2 & 110.2 & & & \\ 111.2 & 268.4 & 111.0 & & & \\ 110.2 & 111.0 & 267.2 & & & \\ & & & 79.06 & & \\ & & & & 78.72 & \\ & & & & & 78.85 \end{bmatrix}$$

$$S_{ij} = \begin{bmatrix} 0.0049165 & -0.0014470 & -0.0014266 & & & \\ -0.0014470 & 0.0049245 & -0.0014490 & & & \\ -0.0014266 & -0.0014490 & 0.0049328 & & & \\ & & & 0.0126486 & & \\ & & & & 0.0127033 & \\ & & & & & 0.0126823 \end{bmatrix}$$

ABAQUS software requires specifying the nine elastic engineering constants in the following sequence: E_1, E_2, E_3, ν_{12}, ν_{13}, ν_{23}, $G12$, $G13$, $G23$. Using the crystallites orientations obtained by CA computation, the martensite orthotropic elasticity of weld DP600 can be defined using specific formula defining the influence of orientation angle. Thus the figure 5 pictures the crystalline growth simulated by CA method. From the edge of the weld the crystallites pool gradually grow to the center weld pool. Because these crystallites grow faster than the others along a preferential direction, starting from the orientation's distribution obtained by CA model, it can be observed that the preferred orientation is around of $\theta = 37.54^{\circ}$ with respect to the welding direction.

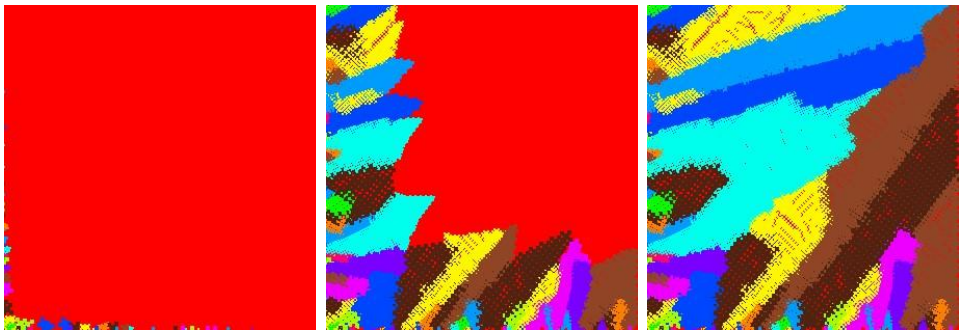

(a) 206 CA step (b) 721 CA step (c) 1774 CA step

Figure 5. Crystallites growth simulation obtained by the CA model

If the orthotropic elastic stiffness of original martensite in the initial coordinate system A is defined by $[C_{ij}^{A}]$, the orthotropic elastic stiffness of the rotated martensite noted by $[C_{ij}^{B}]$ corresponding to the coordinate system B (defined by an orientation angle θ chosen in the plate plane) can be computed from the following formulas:

$$[C_{ij}^{B}] = [\alpha_{ij}]^{-1}[C_{ij}^{A}][\beta_{ij}] \tag{4}$$

where the matrix of $[\alpha_{ij}]^{-1}$ and $[\beta_{ij}]$ can be given by:

$$[\alpha_{ij}]^{-1} = \begin{bmatrix} cos^2\theta & sin^2\theta & & 2sin\theta cos\theta \\ sin^2\theta & cos^2\theta & & -2sin\theta cos\theta \\ & & 1 & \\ & & cos\theta & -sin\theta \\ & & sin\theta & cos\theta \\ -sin\theta cos\theta & sin\theta cos\theta & & cos^2\theta - sin^2\theta \end{bmatrix} \tag{5}$$

$$[\beta_{ij}] = \begin{bmatrix} cos^2\theta & sin^2\theta & -sin\theta cos\theta \\ sin^2\theta & cos^2\theta & sin\theta cos\theta \\ & & 1 \\ 2sin\theta cos\theta & -2sin\theta cos\theta & cos\theta \quad sin\theta \\ & & -sin\theta \quad cos\theta \\ & & cos^2\theta - sin^2\theta \end{bmatrix} \quad (6)$$

The cosines components of the rotation matrix defining relationships between the x, y, z axis coordinates of A x_A, y_A, z_A and x, y, z axis coordinates of B x_B, y_B, z_B are shown in table 2:

Table 2. Cosines values defining a plane rotation with the angle θ

	x_A	y_A	z_A
x_B	cos θ	-sinθ	0
y_B	sin θ	cos θ	0
z_B	0	0	1

Concerning the temperature influence on all elastic constants firstly is considered a proportional variation with the DP600 base metal Young's modulus and Poisson's modulus defined in table 1. A linear interpolation is applied to decrease the elastic constants proportionally with the temperature increases: 300℃, 600℃ and 800℃ using the following formulas:

$$\frac{W_T}{W_0} = \frac{B_T}{B_0} \quad (7)$$

Here W_T stands the weld material Young's Modulus and Poisson's ratio values of E_1, E_2, E_3, ν_{12}, ν_{13}, ν_{23}, G_{12}, G_{13} and G_{23} at temperature T (0℃, 300℃, 600℃ and 800℃) and B_T stands for the corresponding base material Young's Modulus and Poisson's ratio values of Table 1.

Using the interpolation relationship (7) the elastic coefficients values corresponding to the original martensitic compliance matrix $[S_{ij}^A] = [C_{ij}^A]^{-1}$ defined in the initial orthotropic coordinates system A are shown in Table 3.

Table 3. Elastic constants of weld material computed from C_{ij} matrix of martensite (GPa)

T/℃	E_1	E_2	E_3	υ_{12}	υ_{13}	Y_{23}	G_{12}	G_{13}	G_{23}
0	203.40	203.07	202.72	0.2943	0.2902	0.2942	79.06	78.72	78.85
300	184.03	183.73	183.42	0.3101	0.3057	0.3100	71.53	71.22	71.34
600	116.23	116.04	115.84	0.3258	0.3213	0.3258	45.18	44.98	45.06
800	29.06	29.01	28.96	0.3469	0.3420	0.3468	11.29	11.25	11.26

Using formula (4), (5) and (6) it is computed the elastic compliance matrix corresponding to the preferred crystallites orientation and all obtained parameters (Table 4) are input into the Abaqus FEM.

Table 4. Elastic constants of weld material computed from preferred crystallites orientation (GPa)

T/℃	E_1	E_2	E_3	υ_{12}	υ_{13}	Y_{23}	G_{12}	G_{13}	G_{23}
0	203.78	203.70	202.72	0.2924	0.2924	0.2935	78.93	78.85	78.85
300	184.37	183.30	183.42	0.3080	0.3081	0.3092	71.42	71.34	71.07
600	116.45	116.40	115.84	0.3237	0.3237	0.3249	45.10	45.05	44.88
800	29.11	29.10	28.96	0.3446	0.3446	0.3459	11.28	11.26	11.22

3.2 Analysis of base metal plastic anisotropy

Based on experimental tensile tests and using formula of plane plastic anisotropic theory, Lankford coefficients and Hill's coefficients of DP600 base metal steel are presented in Table 5 [12]:

Table 5. Lankford coefficients and Hill parameters concerning DP600 base metal

r_0	$r45$	$r90$	R_{11}	R_{22}	R_{33}	R_{12}	F	G	H	N
1.0123	0.6487	0.9160	1	0.9748	0.9777	1.1172	0.5492	0.4969	0.5031	1.2017

4 Analysis of strain rate sensitivity

The hardening term $H(\varepsilon_p)$ of material plastic flow can only predict the rheological behavior at a particular strain rate. For materials undergoing temperature variations a strain rate sensitivity analysis must be add to predict more precisely the corresponding flow stress changes. The temperature sensitivity *F(T)* under room temperature is set to 1 and a reference material strain rate $\dot{\varepsilon}_0 = 1$ is chosen. Starting from the strain rate sensitivity function $G(\dot{\varepsilon})$ proposed by A. Gavrus [13,14] physically based on kinetics of dislocations glide, available simultaneously for both static or dynamic conditions and for materials undergoing important strain rate gradients, the below expression is used:

$$G(\dot{\varepsilon}) = 1 + Ash\left[\frac{1}{2}\left(\frac{\dot{\varepsilon}}{\dot{\varepsilon}_0}\right)^D\right] \tag{8}$$

Concerning the dual-phase D600 steel the visco-plastic constitutive model can be written from general rheological law of A. Gavrus [13,14] and previous work of S. Liu et al [12], considering an Avrami mixture formulation based on plastic strain hardening of martensite, dynamic recovery of ferrite, temperature influence and strain rate sensitivity using the following equation:

$$\sigma\left(\varepsilon_p, T, \dot{\varepsilon}\right) = H\left(\varepsilon_p\right) \cdot F(T) \cdot G(\dot{\varepsilon}) = \left\{w \cdot \left(\sigma_y + n_1 {\varepsilon_p}^{n_2}\right) + (1-w) \cdot \left[\sigma_y + n_3\left(1 - e^{-n_4 \varepsilon_p}\right)\right]\right\} \cdot (1 - k \cdot T^{*m})^n \cdot p \cdot \{1 + Ash\left[\frac{1}{2}\left(\frac{\dot{\varepsilon}}{\dot{\varepsilon}_0}\right)^D\right]\} \tag{9}$$

The hardening of martensite is described using a Ludwick law, the softening of ferritic phase is described by a Voce model and the dual-phase mixture by a dynamic Avrami formulation. According to the Eq. 9 and using the experimental true stress–plastic strain tensile data obtained at room temperature (Figure 6), the corresponding identified parameters are presented in Table 6.

Table 6. Parameter identification results of DP600 plastic constitutive behavior at room temperature

w^*	σ_y	n_1	n_2	n_3	n_4
0.2	331.74	2772.93	0.5765	621.08	11.5505
k	m	n	p	$\dot{\varepsilon}_0$	D
0.49	4.21	103.17	0.7023	1	0.0160537

*martensite fraction corresponding to the dual phase (ferrite-martensite) DP600 steel (here w=0.2)

It is shown from the flow stress curves plotted in figure 6 that the identified material plasticity model of dual-phase DP600 steel predicts well the hardening and strain rate sensitivity.

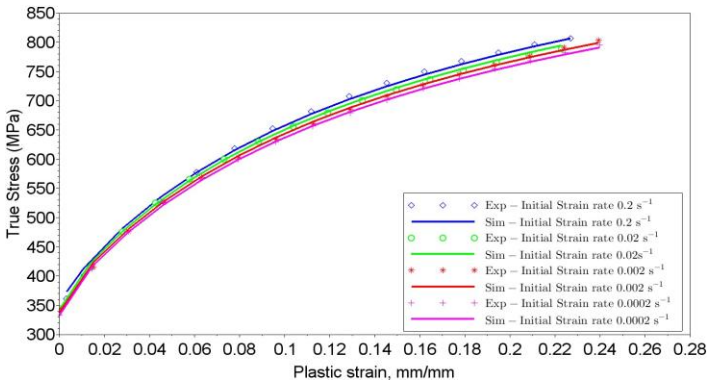

Figure 6. Comparison between experimental tensile flow stress curve at room temperature and the identified thermo-mechanical plastic constitutive model

5 Numerical Results

5.1 Analysis of weld elastic anisotropy influence

Figure 7 plotted the equivalent residual stresses variation along the transversal path (see figure 3) for the three material models: DP600 base metal model, weld model using material orientation along welding direction and weld model using material orientations obtained by CA model. The mainly difference between the three models is caused principally by the material elasticity properties. As is described at section 3.1, DP600 base metal model use the reference metal elasticity for all material zones (FZ, HAZ, BM), while the named weld model uses a weld material elasticity in the fusion region (FZ). Nearly no differences are found on the residual stresses between the DP600 base model and the weld model using orientations along welding direction. By introduction of weld material orientations simulated by CA model, the numerical results on residual stresses are about 50 MPa reduced around the weld zone. These results show that the difference of the elasticity considering ferrite-martensite transition has little influence on residual stresses in numerical simulation of dual phase steel DP600 laser welding. Moreover the elasticity differences considering crystals orientations of weld material can reduce the residual stresses around the weld.

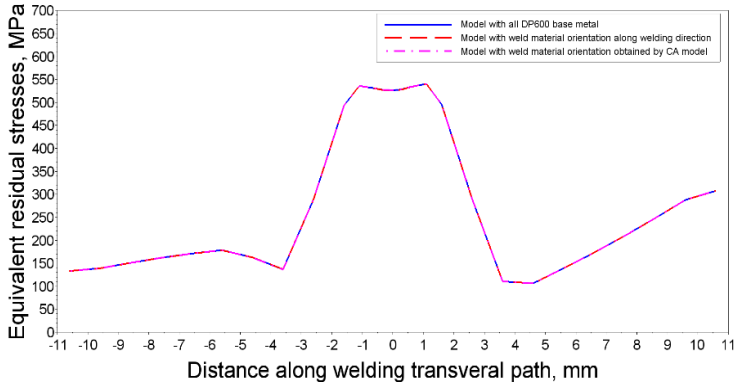

Figure 7. Numerical simulation results of Von-Mises residual stresses using three elasticity models

5.2 Analysis of base metal plastic anisotropy influence

Different plate welding orientations θ = 0°, 30°, 45°, 60° and 90° with material rolling direction are used to simulate welding process. The FEM numerical results concerning Hill'48 [15] equivalent

residual stresses along transversal path are presented in figure 8. It can be observed that the material rolling orientation influences the magnitude of equivalent Hill residual stresses around the weld.

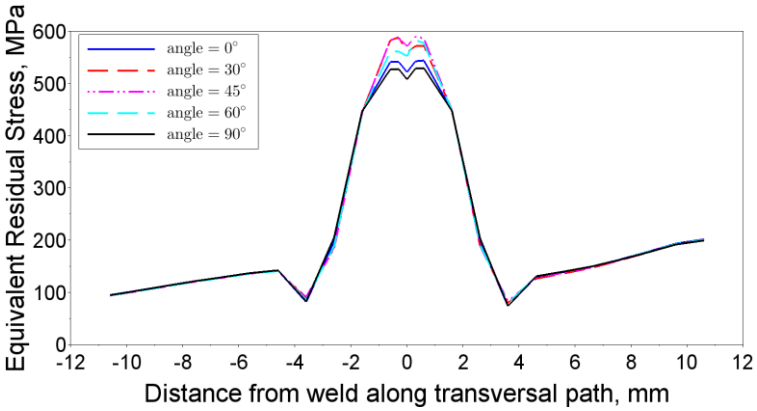

Figure 8. Numerical Hill residual stresses obtained from different orientations of the welding with the plate rolling direction

5.3 Analysis of strain rate sensitivity influence

Equivalent stresses and effective plastic strains (PEEQ) distributions and corresponding values along welding longitudinal and transversal path using FEM simulations with and without strain rate sensitivity are compared and presented in figure 9 and 10. The numerical results show a general small sensitivity of the strain rate term. However a particular important rise of the PEEQ and equivalent residual stresses occur on the weld center area.

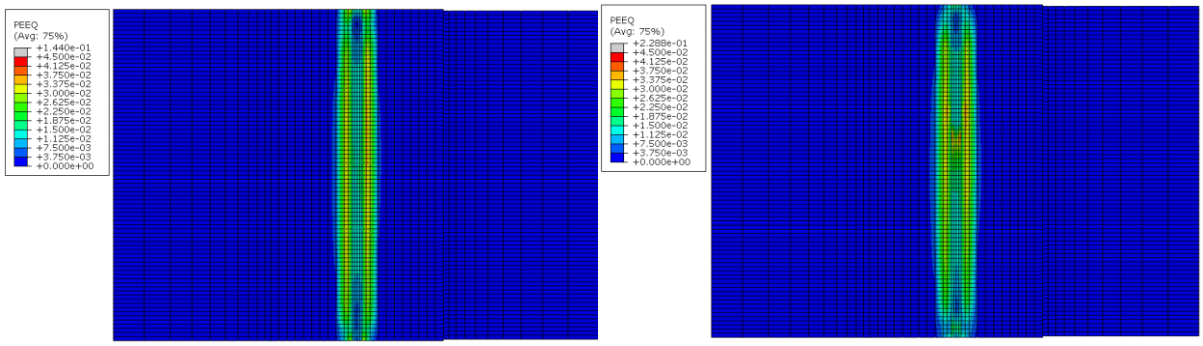

(a) (b)

Figure 9. Numerical iso-values of effective plastic strains (PEEQ) distribution: a) without strain rate sensitivity term, b) with strain rate sensitivity term

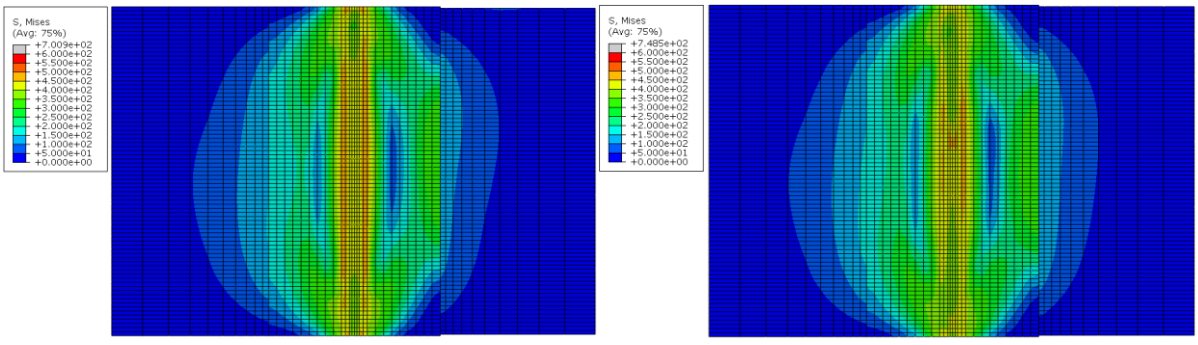

(a) (b)

Figure 10. Numerical iso-values of Hill equivalent stress distribution: a) without strain rate sensitivity term, b) with strain rate sensitivity term

Furthermore comparisons of effective plastic strains variations pictured in figure 11 show that strain rate sensitivity has little influence along a transversal welding path (with a maximum of 30% rise on the welding center), but a relatively important effect (200%) particularly on the edge and middle part along the longitudinal welding direction.

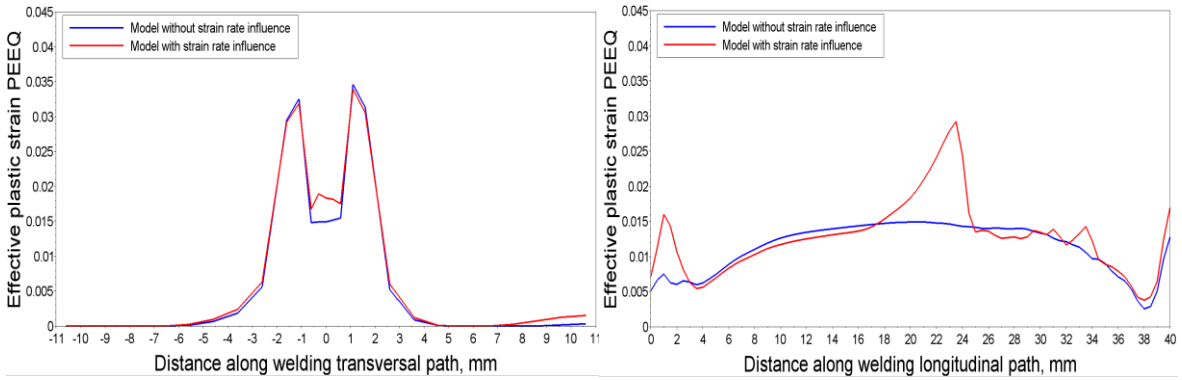

(a) (b)

Figure 11. Effective plastic strains (PEEQ) variations obtained by numerical simulations: a) along transversal welding path, b) along longitudinal welding path

Concerning the Hill equivalent residual stresses variations along the transversal and longitudinal welding path (figure 12) a little influence of the strain rate is again observed excepting the center welding region where a difference around of 20% occurs.

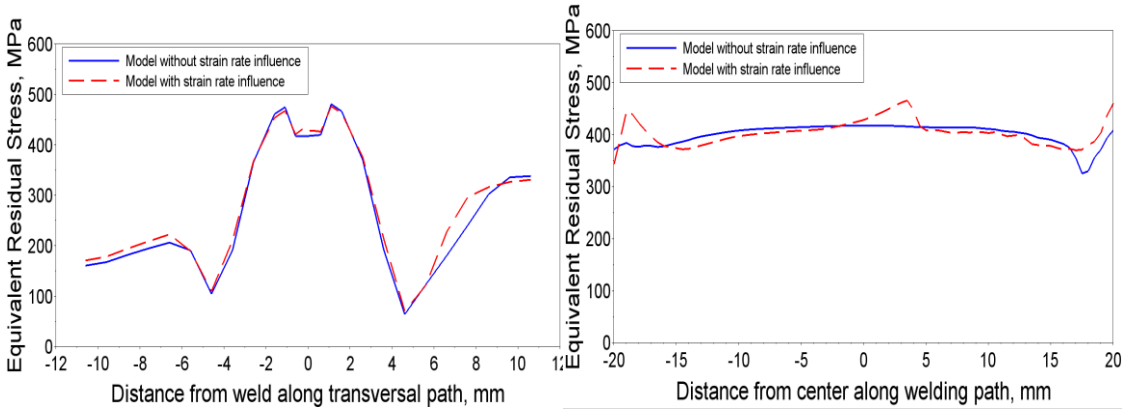

(a) (b)

Figure 12. Hill equivalent residual stresses variations obtained by numerical simulations: a) along transversal welding path, b) along longitudinal welding path

6 Conclusions

All the obtained numerical results of this study lead to a better understanding of the correlations between the laser welding process and the welding microstructure, residual stresses and global weld quality in the case of a dual-phase DP600 steel. The analysis of the proposed simulation model can draw three major conclusions.

1. Concerning the influence of weld elastic anisotropy the equivalent residual stresses along transversal path of base metal elasticity model and weld elasticity model have been compared.

The difference of elasticity models considering ferrite-martensite transition and crystalline orientation influences the numerical residual stresses only in the central welding region.

2. Concerning the base metal plastic anisotropy influence, laser welding processes defined by different orientations with respect to the material rolling have been simulated. The results of equivalent residual stresses show that the plastic material anisotropy influence the magnitude of longitudinal and transversal residual stresses around the weld.
3. To improve material plastic flow especially for a wide range of temperatures (from room temperature to fusion temperature), a strain rate sensitivity model has been identified based on experimental DP600 true stress-plastic strain tensile curves obtained at 20°C and on a modified Johnson-Cook temperature sensitivity term. As a first approximation, the strain rate sensitivities for high temperatures have been supposed in this work to be the same as that for room temperature. It has been shown from the obtained numerical results of FEM simulations taking into account a material strain rate constitutive behavior that the plastic strains and equivalent residual stresses have similar global variations as compared with a FEM model without a strain rate sensitivity term. However pronounced peaks with higher values were observed at the beginning, center and end of the weld in the case of use of strain rate sensitivity.

Acknowledgement

The work was financially supported by China Scholarship Council and GCGM laboratory of INSA Rennes.

References

[1] Geoffrey Davies, Materials for automobile bodies, Butterworth Heinemann, 2012.

[2] Marion Calcagnotto, Yoshitaka Adachi, Dirk Ponge, and Dierk Raabe, Deformation and fracture mechanisms in fine-and ultrafine-grained ferrite/martensite dual-phase steels and the effect of aging, Acta Materialia, 59(2) (2011) 658–670.

[3] Shuang Kuang, Yong-lin Kang, Hao Yu, and Ren-Dong Liu, Effect of continuous annealing parameters on the mechanical properties and microstructures of a cold rolled dual phase steel, International Journal of Minerals, Metallurgy and Materials 16(2) (2009) 159–164.

[4] O. Bouaziz, H. Zurob, and M. Huang, Driving force and logic of development of advanced high strength steels for automotive applications. Steel Res. Int., 84(10) (2013) 937–947.

[5] Fraunhofer CLA, Making innovation a reality, Meet Fraunhofer IWS and Fraunhofer CCL's Laser Applications Division at LME.

[6] N. Farabi, D. L. Chen, J. Li, Y. Zhou, and S. J. Dong, Microstructure and mechanical properties of laser welded dp600 steel joints, Materials Science and Engineering A 527(4–5) (2010) 1215–1221.

[7] Danyang Dong, Yang Liu, Yuling Yang, Jinfeng Li, Min Ma, and Tao Jiang, Microstructure and dynamic tensile behavior of DP600 dual phase steel joint by laser welding, Materials Science and Engineering A 594 (2014) 17–25.

[8] Y Y Zhao, Y S Zhang, and W Hu, Effect of welding speed on microstructure, hardness and tensile properties in laser welding of advanced high strength steel, Science and Technology of Welding and Joining 18(7) (2013) 581–590.

[9] Mingsheng Xia, Elliot Biro, Zhiling Tian, and Y. Norman Zhou, Effects of heat input and martensite on haz softening in laser welding of dual phase steels, ISIJ International 48(6) (2008) 809–814.

[10] N. Farabi, D. L. Chen, and Y. Zhou, Microstructure and mechanical properties of laser welded dissimilar dp600/dp980 dual-phase steel joints, J. of Alloys and Compounds 509(3) (2011) 982–989.

[11] Sudook A. Kim and Ward L. Johnson, Elastic constants and internal friction of martensitic steel, ferritic-pearlitic steel, and α-iron, Mat. Sci. and Eng. A 452-453 (2007) 633–639.

[12] S. Liu, A. Kouadri-Henni, and A. Gavrus, Numerical simulation and experimental investigation on the residual stresses in a laser beam welded dual phase DP600 steel plate: Thermo-mechanical material plasticity model, Int. J. Mech. Sci. 243 (2017) 122:235.

[13] A. Gavrus, Formulation of a new constitutive equation available simultaneously for static and dynamic loadings, DYMAT Int. Conf. on the Mechanical and Physical Behaviour of Materials under Dynamic Loading, EDP Science, Bruxelles, Belgium, 2009, pp. 1239-1244.

[14] Adinel Gavrus, Constitutive equation for description of metallic materials behavior during static and dynamic loadings taking into account important gradients of plastic deformation, Key Engineering Materials 504 (2012) 697-702.

[15] Hill, R. A theory of the yielding and plastic flow of anisotropic metals. In: Proc. of the Royal Society of London A: Math., Phys. Eng. Sci.. Vol. 193. The Royal Society, pp. (1948) 281-297.